Chester supersolid of spatially indirect excitons in double-layer semiconductor heterostructures

Chester supersolid of spatially indirect excitons in double-layer semiconductor heterostructures

Sara Conti[1], Andrea Perali[2], Alexander R. Hamilton[3], Milorad V. Milošević[1,4], François M. Peeters[1,5], and David Neilson[1,3]
[1]*Department of Physics, University of Antwerp, 2020 Antwerp, Belgium*
[2]*Supernano Laboratory, School of Pharmacy, University of Camerino, 62032 Camerino (MC), Italy*
[3]*ARC Centre of Excellence for Future Low Energy Electronics Technologies, School of Physics, University of New South Wales, Sydney 2052, Australia*
[4]*NANOlab Center of Excellence, University of Antwerp, 2020 Antwerp, Belgium*
[5]*Universitade Federal do Ceara, Departamento de fisica, 60455-760 Fortaleza, Brasil*

A supersolid, a counter-intuitive quantum state in which a rigid lattice of particles flows without resistance, has to date not been unambiguously realised. Here we reveal a supersolid ground state of excitons in a double-layer semiconductor heterostructure over a wide range of layer separations outside the focus of recent experiments. This supersolid conforms to the original Chester supersolid with one exciton per supersolid site, as distinct from the alternative version reported in cold-atom systems of a periodic density modulation or clustering of the superfluid. We provide the phase diagram augmented by the supersolid. This new phase appears at layer separations much smaller than the predicted exciton normal solid, and it persists up to a solid–solid transition where the quantum phase coherence collapses. The ranges of layer separations and exciton densities in our phase diagram are well within reach of the current experimental capabilities.

The existence of supersolid phases has attracted interest for a long time, as it is intriguing and rather counter-intuitive to attempt to visualize particles flowing without resistance while they form a rigid lattice [1]. In this exotic phase, spatial off-diagonal long-range order and periodic solid order coexist, spontaneously breaking particle conservation and continuous translational invariance [2]. Chester [3] originally proposed a supersolid ground state of ^{4}He, with a single atom localized at each lattice site of the ^{4}He crystal. There have been some indications of this phase in ^{4}He in torsional-oscillator experiments from non-classical rotational inertia [4], but it appears that condensate fractions will be disappointingly tiny [5].

Alternative approaches to forming a supersolid have involved quantum gases of cold atoms in optical lattices [6], with recent reports of observations of supersolid phases [7–10], and ultra-cold dipolar excitons, with reports of a macroscopically ordered exciton state [11, 12]. However one must distinguish these periodic density-modulated or clustered condensates, with the Chester concept of supersolidity where simultaneously within the macroscopic quantum condensate, there is a single particle localized on each lattice site by strong interparticle repulsion, in analogy with ^{4}He.

Here we show that excitons in a semiconductor heterostructure can form a supersolid of the Chester type, with a single exciton at each site of the supersolid lattice without vacancies. The heterostructure consists of parallel p-doped and n-doped conducting layers. The electrons and holes are spatially confined in their layers by an insulating barrier of thickness d and dielectric constant ϵ. The equal carrier densities ρ can be tuned by top and bottom metal gates. When the average separation between carriers in each layer is much larger than d, the electrons and holes will form bound excitonic-like states aligned perpendicular to the layers. Unlike cold atoms, solidification in this system is driven purely by the repulsion between excitons, the strength of which is tunable by d, ρ, and ϵ. We seek supersolidity at low densities and large layer separations where the exciton-exciton repulsion is strong.

This requirement is realizable in a variety of existing semiconductor systems that are the subject of intense experimental interest due to the accumulating evidence that they support electron-hole superfluidity and Bose-Einstein Condensation, such as double monolayer transition metal dichalcogenides (TMD) [13, 14], Si/Ge heterojunctions [15], double bilayer graphene [16, 17], and double quantum wells in III-V semiconductor heterostructures [18, 19]. Much effort in these systems has focused on achieving very small layer separations so the exciton binding energy is large and the exciton-exciton interaction is weak. In contrast, our supersolid forms at larger interlayer spacing, which is more experimentally accessible.

We determine the zero-temperature phase diagram as a function of the system parameters, the layer separation d and the density ρ with characteristic length $r_0 = 1/\sqrt{\pi\rho}$. The Hamiltonian for the electron-hole pairs is

$$H = \sum_{i=1}^{N} \left(-\frac{\hbar^2}{2M_{\rm X}} \right) \nabla_i^2 + \sum_{i<j=1}^{N} V_{\rm XX}(|\mathbf{r}_i - \mathbf{r}_j|) \,. \quad (1)$$

The index i labels the N exciton pairs of mass $M_{\rm X}$ at positions $\mathbf{r}_i$ parallel to the layers. For convenience, we take equal electron and hole masses, $m_e^* = m_h^*$. The interaction $V_{\rm XX}(r)$ between two exciton pairs,

$$V_{\rm XX}(r) = \frac{1}{4\pi\epsilon} \frac{e^2 d^2}{r(r^2+d^2)} \,, \quad (2)$$

contains the four Coulomb interactions acting between the electrons and holes forming the pairs.

Next we introduce variational functions for the many-particle states. To determine the ground state, we minimize the energy for (i) the order parameter of the superfluid phase, (ii) the wave function of the exciton normal solid, and (iii) the order parameter of the exciton supersolid.

(i) The BEC order parameter of the superfluid is [20],

$$\langle \hat{\Phi}_{sf}^{\dagger}(\mathbf{r}) \rangle = \Phi_{sf}(\mathbf{r}) = \sqrt{\rho} \,, \quad (3)$$

normalized to $\int d^2\mathbf{r}\ |\sqrt{\rho}\,|^2 = N$. $\hat{\Phi}^\dagger_{sf}(\mathbf{r})$ creates an exciton-like boson at position $\mathbf{r}$. We can use the order parameter for the BEC regime because screening suppresses the superfluidity at high density well before it enters the BCS regime [16].

(ii) For the exciton normal solid, the variational wave function is taken as a product of normalized Gaussians, each centered on a different lattice site $\mathbf{a}_i$ of the exciton solid

$$\Phi_{ns}(\mathbf{r}_1,\ldots,\mathbf{r}_N) = \prod_{i=1}^{N} \frac{1}{\sqrt{\pi}\sigma_{ns}} \mathrm{e}^{-(\mathbf{r}_i-\mathbf{a}_i)^2/2\sigma_{ns}^2}\ , \quad (4)$$

with variational parameter σ_{ns}. The N sites $\{\mathbf{a}_i\}$, equal to the number of excitons, form a triangular lattice [21] with lattice constant a determined by the exciton density, $\rho = 2/(\sqrt{3}a^2)$. For a stable solid, $\sigma_{ns} \ll a$.

(iii) For the exciton supersolid we choose a form for the variational BEC order parameter $\Phi_{ss}(\mathbf{r})$ [22] that corresponds to exactly one exciton per supersolid site, and contains phase coherence on the macroscopic scale,

$$\langle\hat{\Phi}^\dagger_{ss}(\mathbf{r})\rangle = \Phi_{ss}(\mathbf{r}) = \sqrt{\rho_{sf}} + \sqrt{\rho_{ss}} \sum_{i=0}^{N} \mathrm{e}^{-(\mathbf{r}-\mathbf{a}_i)^2/2\sigma_{ss}^2}\ . \quad (5)$$

Equation (5) represents a phase coherent state as it is evident that the corresponding one-body density matrix,

$$\langle\hat{\Phi}^\dagger_{ss}(\mathbf{r})\,\hat{\Phi}_{ss}(\mathbf{r}')\rangle = N(\sqrt{\rho_{sf}} + \sqrt{\rho_{ss}}\sum\nolimits_i \mathrm{e}^{-(r-a_i)^2/2\sigma_{ss}^2}) \times (\sqrt{\rho_{sf}} + \sqrt{\rho_{ss}}\sum\nolimits_j \mathrm{e}^{-(r'-a_j)^2/2\sigma_{ss}^2}), \quad (6)$$

does not vanish when $|\mathbf{r}-\mathbf{r}'| \to \infty$, and so has off-diagonal long-range order (ODLRO) [23]. At the same time, $\Phi_{ss}(\mathbf{r})$ and $\Phi_{ns}(\mathbf{r}_1,...,\mathbf{r}_N)$ share identical diagonal long-range order from the symmetry of the triangular lattice $\{\mathbf{a}_i\}$ [24–26].

The normalization of the supersolid order parameter, $\int d^2\mathbf{r}\ |\Phi_{ss}(\mathbf{r})|^2 = N$, ensures that there is only one exciton per supersolid site. Thus it is not a density wave. There are two independent variational parameters: the localization parameter σ_{ss}, and the spatially homogeneous background component ρ_{sf}. The parameter ρ_{ss} is fixed by the normalization.

A stable supersolid requires $0 < \rho_{sf} < \rho$. When $\rho_{sf} = 0$, $\Phi_{ss}(\mathbf{r})$ cannot be lower in energy than $\Phi_{ns}(\mathbf{r}_1,\ldots,\mathbf{r}_N)$, because the ODLRO in $\Phi_{ss}(\mathbf{r})$ associated with the additional overlaps of the Gaussians pushes up the exciton-exciton interaction energy [22]. The other limit, $\rho_{sf} = \rho$, gives $\rho_{ss} = 0$, so $\Phi_{ss}(\mathbf{r})$ reverts to $\Phi_{sf}(\mathbf{r})$ for the superfluid.

We calculate the energies $\langle H\rangle$ for the three phases with the wave functions given by Eqs. (3) – (5). To take into account the short range two-body correlations that are expected to be strong in the low-density region where we work, in evaluating the expectation value $\langle V_{XX}\rangle$ of the interaction we set $\Phi^\dagger(\mathbf{r})\Phi^\dagger(\mathbf{r}')V_{XX}(\mathbf{r}-\mathbf{r}')\Phi(\mathbf{r})\Phi(\mathbf{r}') = 0$ when $|\mathbf{r}-\mathbf{r}'| < R_c$. This takes into account the vanishing of the pair correlation function at small r for low densities [27]. We determine R_c by matching our results with the position of the exciton superfluid to normal-solid transition obtained from quantum Monte Carlo (QMC) [24, 25]. The resulting value $R_c \sim 0.9r_0$ is consistent with the short-range correlation length scales determined for repulsive dipolar bosons [26]. The short range two-body correlations for the supersolid should be similar to the normal solid, so we use this R_c throughout. We use the effective Bohr radius, $a_B = \hbar^2\epsilon/e^2m^*_e$, as a length scale, and effective mRydberg (mRy*) for energies. In double TMD monolayers, typically $a_B \sim 0.6$ nm and mRy$^* \sim 0.2$ meV.

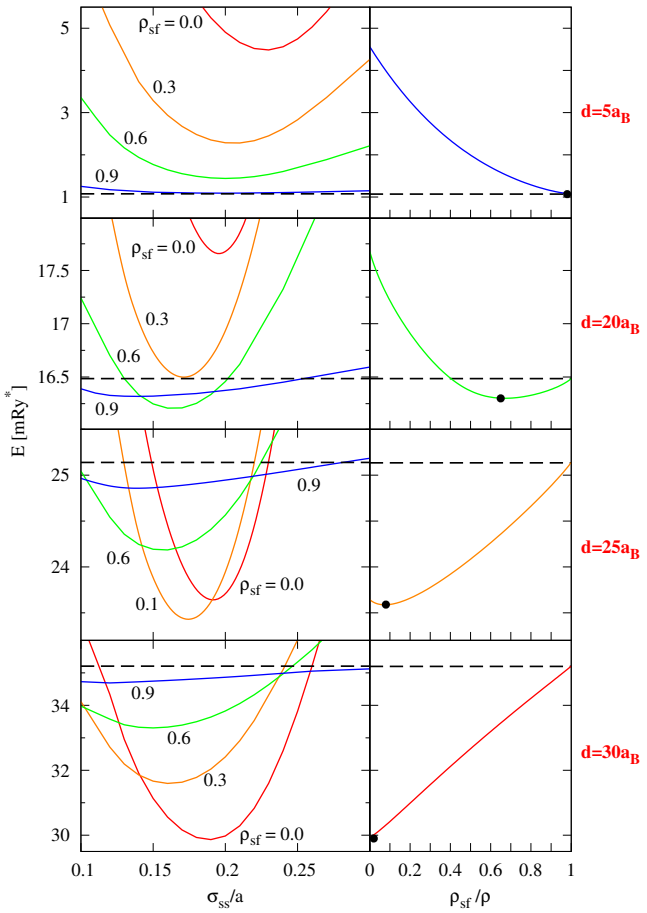

Figure 1. Exciton supersolid energy E_{ss} for layer separations d as indicated for a fixed density at $r_0 = 30a_B$. Dashed line shows for reference the superfluid energy E_{sf}. Left panels: E_{ss} as a function of the localization parameter σ_{ss}/a, for fixed values of the background component ρ_{sf}/ρ as labelled. Right panels: minimum in σ_{ss} of E_{ss} (cf. left panels), plotted as a function of the background component ρ_{sf}/ρ. The dots highlight the absolute minimum of E_{ss}.

Figure 1 compares the supersolid energy E_{ss} (solid lines) with the superfluid energy E_{sf} (dashed lines), for layer separations d at a fixed density corresponding to $r_0 = 30a_B$. E_{ss} is shown as a function of the two variational parameters for the supersolid, ρ_{sf}/ρ and σ_{ss}/a. We recall that, by definition, $E_{ss} = E_{sf}$ when $\rho_{sf}/\rho = 1$.

For the smallest layer separation shown, $d = 5a_B$, the minimum in E_{ss} as a function of σ_{ss} increases monotonically as ρ_{sf}/ρ decreases from 1 to 0. The monotonic increase implies that the superfluid energy forms a lower bound on the exciton

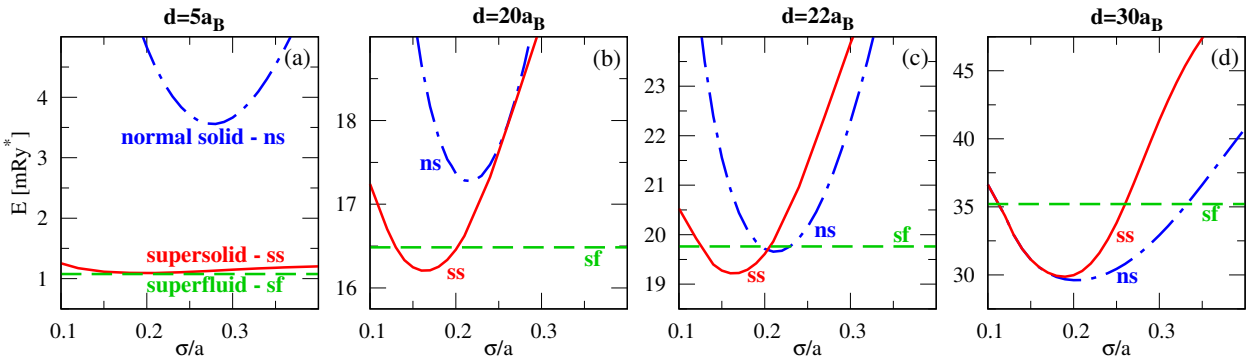

Figure 2. Energies of the superfluid (sf), exciton supersolid (ss) and exciton normal solid (ns) phases, as labelled, for different layer separations d. Density fixed at $r_0 = 30a_B$. The dependence of E_{ss} and E_{ns} on the localization variational parameter, $\sigma = \sigma_{ss}$ or $\sigma = \sigma_{ns}$, is shown. Each E_{ss} curve uses the value of ρ_{sf}/ρ yielding the lowest energy.

supersolid energy. So for $d = 5a_B$, the supersolid is not the ground state. In contrast, for a larger $d = 20a_B$, the minimum in E_{ss} as a function of σ_{ss} first decreases as ρ_{sf} decreases from 1. It drops below E_{sf}, reaching a lowest value at $\rho_{sf}/\rho = 0.6$. Thus, the exciton supersolid is more stable than the superfluid for $d = 20a_B$. As d is further increased, this minimum in E_{ss} reaches a lowest value at smaller values of ρ_{sf}/ρ. By $d = 25a_B$, the minimum is at $\rho_{sf}/\rho = 0.1$, and by $d = 30a_B$ it decreases monotonically. Again, for these cases the supersolid is more stable than the superfluid.

Figure 2 shows for the same density as Fig. 1, the energies of the exciton superfluid E_{sf}, supersolid E_{ss}, and normal solid E_{ns} phases. The dependence of E_{ns} on $\sigma = \sigma_{ns}$ and E_{ss} on $\sigma = \sigma_{ss}$ is plotted. Each E_{ss} curve uses the value of ρ_{sf}/ρ yielding the lowest energy (Fig. 1). For $d = 5a_B$, the minimum of E_{ns} lies above E_{sf}, so the superfluid is the ground state. By $d = 20a_B$, the minimum of E_{ss} has dropped below E_{sf} and it is still below the minimum of E_{ns}, so the supersolid is the ground state. E_{ns} finally touches E_{sf} at $d \simeq 22a_B$ (Fig. 2(c)), matching the position in phase space of the exciton liquid to normal-solid transition predicted by QMC in Ref. [24]. However since for this d the supersolid phase is still the ground state, it preempts this transition. Only when the layer separation is increased to $d = 30a_B$, does the minimum of E_{ns} drop below E_{ss}. This signals an intriguing supersolid to normal-solid transition, in which the ground-state crystal structure is unchanged but the quantum phase coherence collapses. We note that the energies around this density and layer separation, are consistent with QMC calculations [28].

It is interesting to compare in Fig. 2, the dependence of σ/a at the minima of E_{ns} and E_{ss} on the layer spacing. As d increases, the repulsive interaction (Eq. (2)) becomes stronger than the kinetic energy, and the particles should become more localized on their lattice sites, corresponding to a decreasing σ/a. This is clearly visible in the minimum of the normal solid. In contrast for the supersolid, the localization degree σ/a remains notably little changed over this range of d.

Figure 3(a) shows that for the supersolid it is ρ_{sf}/ρ that changes dramatically with d. The figure plots ρ_{sf}/ρ for the

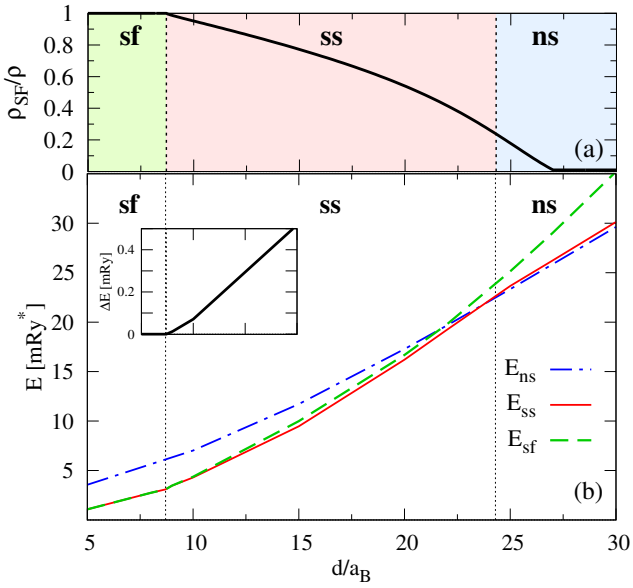

Figure 3. a) Dependence of ρ_{sf}/ρ on separation d for the lowest value of E_{ss}. Colored areas indicate the ground state: sf - superfluid, ss - exciton supersolid, ns - exciton normal solid. b) Minimum superfluid energy E_{sf}, exciton supersolid energy E_{ss}, and exciton normal solid energy E_{ns} as functions of d. The crossings of energies are marked by vertical dotted lines. Inset shows energy difference $\Delta E = E_{sf} - E_{ss}$ on same d scale. Fixed density, with $r_0 = 30a_B$.

lowest E_{ss} as a function of d, for the same density as Fig. 1. The ground states (shaded areas) are extracted from Fig. 3(b), which shows the minima of the energies of the three phases. The two energy crossings, corresponding to the superfluid–supersolid and supersolid–normal solid transitions, are indicated by the dotted lines. For small d, $\rho_{sf}/\rho = 1$ and the superfluid is the ground state. For intermediate values of d, ρ_{sf}/ρ decreases, but before it reaches zero, there is the transition to the normal solid ground state, with its minimum energy dropping below the minimum supersolid energy. We find that for all densities, the supersolid phase is only stable relative

to the normal solid when $\rho_{sf}/\rho \gtrsim 0.25$, confirming that due to the ODLRO, a stable supersolid only exists for non-zero ρ_{sf}/ρ. *In other words, a substantial background component in the supersolid order parameter is necessary to stabilize a Chester-type supersolid.*

Condensation in quantum crystals can occur if there exists an appreciable probability of exchange of particles between adjacent sites[1]. This is only possible when there is an overlap of connected wave functions [1, 5, 29]. In a conventional solid with disconnected wave functions at each lattice site, condensation cannot occur. The exchange can be provided by the presence of defects in the crystal [30, 31], but here it is the spatially homogeneous background component in the order parameter (Eq. (5)) that provides the necessary overlap.

Figure 4 shows the phase diagram. The energies driving the phases are the electron-hole attraction between layers $V_{eh} = -e^2/(4\pi\epsilon\, d)$, the repulsion between charges within each layer $V_{ee} = V_{hh} = e^2/(4\pi\epsilon\, r)$, the exciton-exciton repulsion $V_{\rm XX}$ (Eq. (2)), and the Fermi energy $E_F = \hbar^2/(2m_e^* r_0^2)$ [32].

The dashed line $d = r_0$ divides the phase diagram into a lower region where the average interlayer attraction $\langle V_{eh}\rangle$ is the most important, and an upper region where the average intralayer repulsions $\langle V_{ee}\rangle = \langle V_{hh}\rangle$ are the most important. For $d \ll r_0$, due to the electron-hole attraction V_{eh}, the exciton-exciton repulsion is dipolar, $V_{\rm XX}(r) = e^2 d^2/(4\pi\epsilon\, r^3)$. For $d \gg r_0$, the effect of V_{eh} is negligible and the exciton-exciton repulsion becomes Coulombic, $V_{\rm XX}(r) = 2e^2/(4\pi\epsilon\, r)$.

The phase space region for small separations d and large r_0 where the ground state is superfluid (green area), has been intensively studied theoretically and experimentally [14, 16, 17, 33]. If r_0 is decreased, $V_{eh}/E_F \sim r_0^2/(d\, a_B)$ will decrease, until the superfluid gap generated by V_{eh} drops below E_F. At this point, the strong screening suppresses the superfluid gap so that at $V_{eh}/E_F \simeq 17$ the condensate collapses and there is a transition to the normal-state liquid [33] (green line). Note that the condensate collapse closely follows the Mott exciton dissociation line determined by Ref. [34] for small d/a_B.

At larger d, there is the new supersolid phase occupying a large region of phase space (red area), an intermediate phase lying between the superfluid and normal-solid phases (see also Ref. [35]). The supersolid transition occurs much earlier than the liquid to normal-solid transition predicted at $V_{\rm XX}/E_F = d^2/(r_0 a_B) \simeq 17$ [24, 25] (dotted line). The appearance of the supersolid well below the d predicted for the normal solid is due to the presence of $\rho_{sf} > 0$ in the supersolid order parameter that stabilizes the supersolid phase. This phase persists for $V_{\rm XX}/E_F > 17$, until there is a transition from supersolid to the normal solid (blue area). Further increasing d, we cross $d = r_0$ where $V_{\rm XX}$ becomes Coulombic. Here a low-density bilayer Wigner Crystal ground state has been predicted [28, 36] (yellow area).

We now turn to the melting of the solid phases at high densities. The melting of the bilayer Wigner Crystal was determined in Ref. [28] (orange line). As for the exciton solids, above $d = r_0$ a Coulombic-like $V_{\rm XX}(r)$ cannot support a solid at such high densities. In this way, the exciton normal-solid

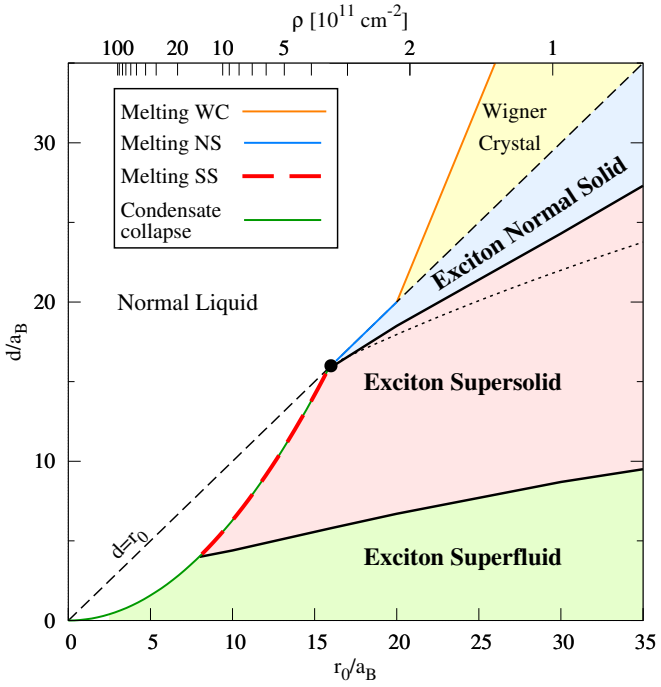

Figure 4. Phase diagram at zero temperature. d is the layer separation and r_0 characterizes the density ρ. Dotted line is the transition to the exciton normal solid predicted in Ref. [24]. Top axis shows densities for a typical double monolayer TMD encapsulated in hBN [14].

melting line is approximately at $d = r_0$ [25] (blue line).

For the supersolid phase there is a second melting mechanism. If the supersolid quantum phase coherence collapses at a d value for which $V_{\rm XX}/E_F < 17$, then the exciton repulsion will not be strong enough to support a normal solid, and so it will melt. The mechanism for this phase coherence collapse is expected to be the same as for the superfluid, that is, a strong increase in the screening. Therefore, we extend the calculation of the superfluid condensate collapse to approximately determine the collapse of the supersolid quantum phase coherence and so the supersolid melting (red line). The approximation is justified both by the resulting supersolid melting line lying close to $d = r_0$, and also because we find the background component ρ_{sf}/ρ in the supersolid is large there.

We note there is a triple point at the intersection of the supersolid melting, the supersolid to normal-solid transition, and the normal-solid melting. The ever present disorder in an experiment will spread the triple point over an area of phase space of co-existing supersolid, normal solid and normal liquid domains, with exciting physics stemming from the diverse and exotic interfaces separating these domains. A fascinating possibility would be Josephson tunneling between supersolid puddles embedded in a normal-state background.

The supersolid melting temperature is determined by the Berezinskii-Kosterlitz-Thouless transition temperature T_{BKT} [37]. Ref. [25] shows T_{BKT} for the superfluid transition and the normal solid melting to be of the order of a few mRy*. We expect the supersolid melting temperature to be of the same

order, corresponding in double TMD monolayers to ~ 2 K.

In conclusion, the supersolid ground state of excitons that we are predicting is robust and extends over a wide area of the equilibrium phase diagram. Since there is precisely one exciton occupying each supersolid site, our supersolid is of the Chester type and fundamentally differs from proposals of supersolids that are superfluids with periodic clustering [31] or periodic density modulation resembling density waves [38].

Intriguingly, we find that a spatially homogeneous background component in the supersolid order parameter is essential to stabilize the Chester-type supersolid, in the absence of other stabilizing factors like vacancies [39] or clustering around the lattice sites [31]. By changing the length of the exciton dipole moment (layer separation) relative to the exciton spacing (density), the exciton-exciton interactions can be tuned to stabilise the superfluid, supersolid, or normal solid. The necessary ranges of densities, layer separations, and dielectric constants are readily accessible experimentally and controllable in semiconductor heterostructures. In addition, our augmented phase diagram offers a rich selection of novel phenomena in the vicinity of the triple point, the solid-solid transition associated with the loss of quantum phase coherence, the supersolid melting coinciding with the condensate collapse, etc., all worthy of further investigation.

We thank Davide Galli, Carlos Sá de Melo and Jacques Tempère for useful discussions. The work was supported by the Flemish Science Foundation (FWO-Vl), and by the Australian Government through the Australian Research Council Centre of Excellence in Future Low-Energy Electronics (Project No. CE170100039).

[1] A. J. Leggett, Can a solid be "Superfluid"?, Phys. Rev. Lett. **25**, 1543 (1970).
[2] S. Balibar and F. Caupin, Supersolidity and disorder, J. Phys.: Cond. Matter **20**, 173201 (2008).
[3] G. V. Chester, Speculations on Bose-Einstein condensation and quantum crystals, Phys. Rev. A **2**, 256 (1970).
[4] E. Kim and M. H. W. Chan, Observation of superflow in solid Helium, Science **305**, 1941 (2004).
[5] D. E. Galli, M. Rossi, and L. Reatto, Bose-Einstein condensation in solid ^{4}He, Phys. Rev. B **71**, 140506(R) (2005).
[6] S. M. Roccuzzo and F. Ancilotto, Supersolid behavior of a dipolar Bose–Einstein condensate confined in a tube, Phys. Rev. A **99**, 041601(R) (2019).
[7] L. Tanzi, S. M. Roccuzzo, E. Lucioni, F. Famà, A. Fioretti, C. Gabbanini, G. Modugno, A. Recati, and S. Stringari, Supersolid symmetry breaking from compressional oscillations in a dipolar quantum gas, Nature (London) **574**, 382 (2019).
[8] M. Guo, F. Böttcher, J. Hertkorn, J. N. Schmidt, M. Wenzel, H. P. Büchler, T. Langen, and T. Pfau, The low-energy Goldstone mode in a trapped dipolar supersolid, Nature (London) **574**, 386 (2019).
[9] G. Natale, R. M. W. van Bijnen, A. Patscheider, D. Petter, M. J. Mark, L. Chomaz, and F. Ferlaino, Excitation spectrum of a trapped dipolar supersolid and its experimental evidence, Phys. Rev. Lett. **123**, 050402 (2019).
[10] F. Böttcher, J.-N. Schmidt, M. Wenzel, J. Hertkorn, M. Guo, T. Langen, and T. Pfau, Transient supersolid properties in an array of dipolar quantum droplets, Phys. Rev. X **9**, 011051 (2019).
[11] L. V. Butov, A. C. Gossard, and D. S. Chemla, Macroscopically ordered state in an exciton system, Nature (London) **418**, 751 (2002).
[12] S. V. Andreev, Fragmented–condensate solid of dipolar excitons, Phys. Rev. B **95**, 184519 (2017).
[13] S. Conti, M. Van der Donck, A. Perali, F. M. Peeters, and D. Neilson, Doping-dependent switch from one- to two-component superfluidity in coupled electron-hole van der Waals heterostructures, Phys. Rev. B **101**, 220504(R) (2020).
[14] L. Ma, P. X. Nguyen, Z. Wang, Y. Zeng, K. Watanabe, T. Taniguchi, A. H. MacDonald, K. F. Mak, and J. Shan, Strongly correlated excitonic insulator in atomic double layers, Nature (London) **598**, 585 (2021).
[15] S. Conti, S. Saberi-Pouya, A. Perali, M. Virgilio, F. M. Peeters, A. R. Hamilton, G. Scappucci, and D. Neilson, Electron-hole superfluidity in strained Si/Ge type II heterojunctions, npj Quantum Mater. **6**, 41 (2021).
[16] A. Perali, D. Neilson, and A. R. Hamilton, High-temperature superfluidity in double-bilayer graphene, Phys. Rev. Lett. **110**, 146803 (2013).
[17] G. W. Burg, N. Prasad, K. Kim, T. Taniguchi, K. Watanabe, A. H. MacDonald, L. F. Register, and E. Tutuc, Strongly enhanced tunneling at total charge neutrality in double-bilayer graphene-WSe_2 heterostructures, Phys. Rev. Lett. **120**, 177702 (2018).
[18] M. Stern, V. Umansky, and I. Bar-Joseph, Exciton liquid in coupled quantum wells, Science **343**, 55 (2014).
[19] S. Saberi-Pouya, S. Conti, A. Perali, A. F. Croxall, A. R. Hamilton, F. M. Peeters, and D. Neilson, Experimental conditions for the observation of electron-hole superfluidity in GaAs heterostructures, Phys. Rev. B **101**, 140501(R) (2020).
[20] L. P. Pitaevskii, Vortex lines in an imperfect Bose gas, Sov. Phys. JETP **13**, 451 (1961), (Zh. Eksp. Teor. Fiz., **40**, 646 (1961)); E. P. Gross, Hydrodynamics of a superfluid condensate, J. Math. Phys. **4**, 195 (1963).
[21] S. Wessel and M. Troyer, Supersolid hard-core bosons on the triangular lattice, Phys. Rev. Lett. **95**, 127205 (2005).
[22] K. Mitra, C. J. Williams, and C. A. R. Sá de Melo, Hexatic, Wigner Crystal, and superfluid phases of dipolar Bosons (2009), arXiv:0903.4655 [cond-mat.other].
[23] C. N. Yang, Concept of off-diagonal long-range order and the quantum phases of liquid He and of superconductors, Rev. Mod. Phys. **34**, 694 (1962).
[24] G. E. Astrakharchik, J. Boronat, I. L. Kurbakov, and Y. E. Lozovik, Quantum phase transition in a two-dimensional system of dipoles, Phys. Rev. Lett. **98**, 060405 (2007).
[25] J. Böning, A. Filinov, and M. Bonitz, Crystallization of an exciton superfluid, Phys. Rev. B **84**, 075130 (2011).
[26] C. Mora, O. Parcollet, and X. Waintal, Quantum melting of a crystal of dipolar bosons, Phys. Rev. B **76**, 064511 (2007).
[27] B. Tanatar and D. M. Ceperley, Ground state of the two-dimensional electron gas, Phys. Rev. B **39**, 5005 (1989).
[28] S. De Palo, F. Rapisarda, and G. Senatore, Excitonic condensation in a symmetric electron-hole bilayer, Phys. Rev. Lett. **88**, 206401 (2002).
[29] C. Cazorla and J. Boronat, Superfluidity versus localization in bulk ^{4}He at zero temperature, Phys. Rev. B **73**, 224515 (2006).
[30] A. F. Andreev and I. M. Lifshitz, Quantum theory of defects in crystals, Sov. Phys. JETP **29**, 1107 (1969), (Zh. Eksp. Teor. Fiz. **56**, 2057 (1969)).
[31] F. Cinti, T. Macrì, W. Lechner, G. Pupillo, and T. Pohl, Defect-

induced supersolidity with soft-core bosons, Nat. Commun. **5**, 3235 (2014).

[32] Y. N. Joglekar, A. V. Balatsky, and S. Das Sarma, Wigner supersolid of excitons in electron-hole bilayers, Phys. Rev. B **74**, 233302 (2006).

[33] P. López Ríos, A. Perali, R. J. Needs, and D. Neilson, Evidence from quantum Monte Carlo simulations of large-gap superfluidity and BCS-BEC crossover in double electron-hole layers, Phys. Rev. Lett. **120**, 177701 (2018).

[34] V. V. Nikolaev and M. E. Portnoi, Mott transition of spatially indirect excitons, in *Nanomodeling*, Vol. 5509, International Society for Optics and Photonics (SPIE (Denver), 2004) pp. 187 – 193.

[35] B. Spivak and S. A. Kivelson, Phases intermediate between a two-dimensional electron liquid and Wigner crystal, Phys. Rev. B **70**, 155114 (2004).

[36] J. Szymański, L. Świerkowski, and D. Neilson, Correlations in coupled layers of electrons and holes, Phys. Rev. B **50**, 11002 (1994).

[37] J. M. Kosterlitz and D. J. Thouless, Ordering, metastability and phase transitions in two-dimensional systems, J. Phys. C: Solid State **6**, 1181 (1973).

[38] D. V. Fil and S. I. Shevchenko, Electron-hole superconductivity, Low Temp. Phys. **44**, 867 (2018); Stationary waves in a superfluid gas of electron-hole pairs in bilayers, Phys. Rev. B **103**, 205419 (2021).

[39] I. L. Kurbakov, Y. E. Lozovik, G. E. Astrakharchik, and J. Boronat, Quasiequilibrium supersolid phase of a two-dimensional dipolar crystal, Phys. Rev. B **82**, 014508 (2010).